Journal of Elasticity (2026) 158:48
https://doi.org/10.1007/s10659-026-10225-0

RESEARCH

Inhomogeneous Sliding Shear Versus Simple Shear in Linear Elasticity

Federico Oyedeji Falope[1] **· Luca Lanzoni**[1] **· Angelo Marcello Tarantino**[1]

Received: 3 June 2026 / Revised: 4 August 2026 / Accepted: 10 August 2026

Abstract
The simplest possible shear deformation is obtained when a face of a block is displaced relative to its opposite parallel face. This sliding shear problem is physically different from the classic simple shear problem. In fact, simple shear produces a homogeneous deformation field, which is necessarily maintained by distributions of tangential stresses applied on the external faces of the block. By contrast, the deformation field generated by sliding shear is inhomogeneous, with the lateral faces of the block always remaining traction-free. Few studies have been conducted on the sliding shear, so it can be asserted that many questions related to this basic problem remain unresolved today. In this paper, the sliding shear problem is formulated within the framework of classical linear elasticity for isotropic materials. However, due to its mathematical complexity, only semi-analytical solutions are provided.

Keywords Linear elasticity · Simple shear · Sliding shear · Shear deformation

Mathematics Subject Classification 74B20 · 74G75 · 74K10

1 Introduction

In sliding shear deformation, the upper horizontal face of a block is displaced parallel to the lower horizontal face, which is held fixed, while the lateral faces of the block are kept traction-free.

The sliding shear problem has many fields of application. In earthquake engineering, the sliding shear model is useful for understanding the failure mechanisms of shear walls and estimating their shear strength (see, for example, Paulay [1], Colotti [2], and Hidalgo et al. [3]).

✉ Luca Lanzoni
luca.lanzoni@unimore.it

Federico Oyedeji Falope
federicooyedeji.falope@unimore.it

Angelo Marcello Tarantino
angelomarcello.tarantino@unimore.it

1 DIEF, Università di Modena e Reggio Emilia, via P. Vivarelli 10, 41125, Modena, Italy

Published online: 19 August 2026

In geology, sliding shear refers to the mechanism of deformation and movement of two masses of rock or soil slipping past each other horizontally or downslope (see, for example, Coward [4], Simpson and De Paor [5], and Mukherjee and Koyi [6]).

In mechanical and materials engineering, sliding shear is used in the design of joints and composite materials to predict load transfer and failure (see, for example, Amirbayat and Hearle [7], Nunes [8], and Dobrzański and Oleksiak [9]).

Slip in robotic grasping concerns patterns and paradigms used, between robot's gripper/fingers and an object, to prevent slippage during manipulation tasks (see, for example, Macefield et al. [10], Dzitac et al. [11], and Zhang [12]).

To the authors' knowledge, although sliding shear has many practical applications, there is no mechanical model available in the literature that is consistent with the physical aspects of the problem, and the simple shear model is often mistakenly used instead.

The concept of shear gained relevance relatively late in the history of continuum mechanics. While Todhunter and Pearson (1886) [13] attributed to Vicat (1831) [14] the first clear discussion of shear in reference to solids, the first consistent definition of simple shear can be attributed to Signorini (1943) [15]. This is because he approached simple shear through a preliminary characterization of all deformations that leave a single plane point-by-point invariant.

For small deformations, a simple shear deformation is defined as an isochoric plane deformation in which parallel planes remain parallel and maintain a constant distance, while translating relative to each other. This deformation is differentiated from a pure shear by the presence of a rigid rotation. On these topics, Truesdell and Toupin (1966) [16] provided a rigorous and well-established foundation. In particular, they assert that "simple shear is the most important and instructive of all special deformations" (pag. 292 of [16]).

Simple shear has been extensively studied, even in finite elasticity. In this context, after the pioneering textbook by Thomson (later Lord Kelvin) and Tait (1867) [17], many interesting contributions have been achieved (see, for example, Rivlin (1948) [18], Horgan and Murphy (2010) [19], Destrade et al. (2012) [20], Nunes and Moreira (2013) [21], Wang and Wu (2014) [22], Thiel et al. (2019) [23], and Falope et al. (2026) [24]).

Let us now illustrate the differences between the sliding shear, mentioned at the beginning of this Section, and the classical simple shear. In the context of linear elasticity, the inhomogeneous deformed configuration generated by the sliding shear is illustrated in Fig. 1, while the homogeneous deformed configuration associated with the simple shear model is shown in Fig. 2. As can be seen from these two figures, even if the horizontal planes are subject to the same prescribed displacement field, the four lateral faces of the cube undergo different deformations. The lateral faces of the cube warp, with out-of-plane displacements, in the case of sliding shear, while these faces remain perfectly flat in the case of simple shear. In the first case, this is a consequence of the fact that the lateral surfaces are unloaded. Instead, in simple shear, to preserve flat surfaces, it is necessary to apply a constant tangential stress field in the two planes $x = \pm a$. This last condition may appear unrealistic in many practical problems.

From a mathematical point of view, the two problems have uniquely different boundary conditions. However, the mixed nature of the boundary conditions for sliding shear significantly complicates the analysis. In fact, with the lateral faces traction-free, the deformation field of the cube for the sliding shear problem is always inhomogeneous. This paper is devoted to sliding shear, which to date does not appear to have been adequately investigated, considering the (inevitable) inhomogeneity of the deformation field and the three-dimensionality of the model in the framework of linear elasticity. This analysis will allow us to accurately derive the shape of a block in its deformed configuration and in particular the warping of the lateral surfaces.

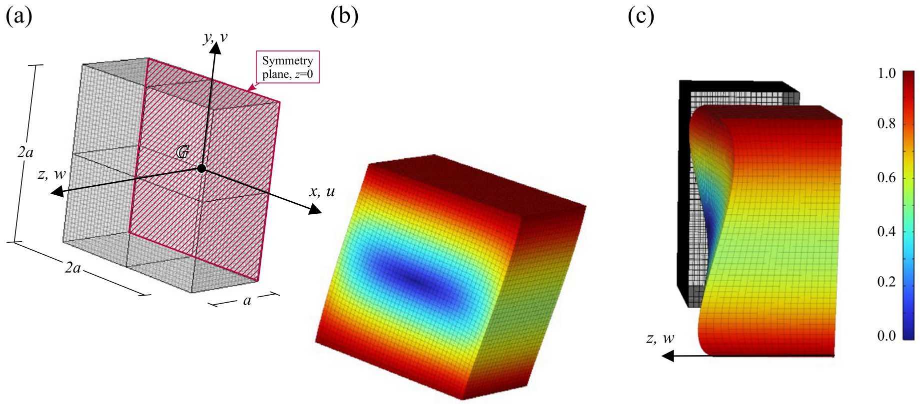

Fig. 1 Sliding shear model. The side surfaces of the cube warp. Given the symmetry only half of the cube is considered. The color maps show the distribution of the displacement, normalized with respect to its maximum values. (a) Undeformed configuration. (b) Deformed configuration. (c) Deformation of the lateral face $z = a$. To visualize the effects, the displacements along the z axis have been considerably increased

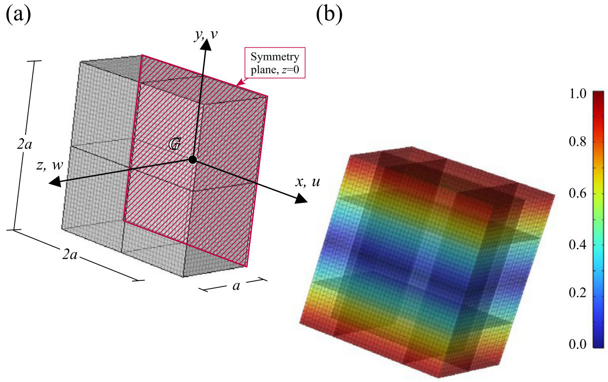

Fig. 2 Simple shear model. The side surfaces of the cube remain flat. Given the symmetry only half of the cube is considered. The color map shows the distribution of the displacement, normalized with respect to its maximum value. (a) Undeformed configuration. (b) Deformed configuration

Even numerical simulations, such as using the Finite Element Method (FEM), do not help to understand the sliding shear problem, as they often provide unrealistically significant stress oscillations near the lateral surfaces.

This paper is organized as follows. Section 2 concerns the mathematical formulation of the sliding shear problem. On the basis of two physical assumptions, the shape of the displacement field is established in Sect. 3. Using the method of separation of variables and Fourier method, series representation for the displacement components are obtained, where unknown constants are present. Using these series in Sect. 4, the stress fields were determined. Boundary conditions are discussed in Sect. 5. To overcome the difficulties due to their mixed nature, a discrete collocation technique is proposed for the computation of the unknown constants. Once these constants have been determined, approximate semi-analytical expressions of the displacement field are derived and, subsequently, strain and stress field are evaluated. Section 6 presents the results obtained for the sliding shear problem. These are then compared with those of the simple shear. Section 7 closes the paper summarizing the results achieved.

2 Problem Formulation

Let us consider a body composed of a homogeneous, isotropic, and linearly elastic material, having the shape of a cube.

Reference is made to a Cartesian coordinate system $\{G, x, y, z\}$ shown in Fig. 1a. Thus, the body can be identified with the closure of the following regular region:

$$\mathcal{B} = \{(x, y, z) \mid -a < x, y, z < a\}$$

of the three-dimensional Euclidean space $\mathcal{E}$. The lengths of the sides of the cube are equal to $2a$. The displacement of a generic material point P can be expressed by the well-known relationship

$$\mathbf{s}(P) = u(P)\mathbf{i} + v(P)\mathbf{j} + w(P)\mathbf{k} \tag{1}$$

where the functions $u(P)$, $v(P)$, and $w(P)$ denote the scalar components of displacement $\mathbf{s}(P)$, whereas $\mathbf{i}$, $\mathbf{j}$ and $\mathbf{k}$ are the unit vectors.

As illustrated in Fig. 1, the sliding shear problem involves the upper face of the cube undergoing a rigid translation in the direction of the x axis. Therefore, the upper face (belonging to the plane $y = a$) remains parallel to the lower one ($y = -a$), which is fixed to the ground. The upper and lower faces of the cube retain their shape, undergoing no pure deformation. All points on the upper plane undergo a rigid displacement along the x axis, which will be denoted by δ_x. To better exploit the symmetry conditions of the deformation with respect to the horizontal plane $y = 0$, the displacement δ_x will be divided in half and applied antisymmetrically to the two horizontal faces of the cube, i.e. $\delta_x/2$ to the upper plane $y = a$ and $-\delta_x/2$ to the lower plane $y = -a$.

The mixed problem of linear elastostatics, which mathematically governs the sliding shear problem, consists in finding the displacement field $\mathbf{s}(P)$, which is the solution of the following partial differential equation (often known as Navier-Lamé equations):

$$\Delta\mathbf{s} + \frac{1}{1-2\nu}\mathrm{Grad}(\mathrm{Div}\mathbf{s}) + \frac{1}{\mu}\mathbf{b} = \mathbf{o}, \tag{2}$$

where $\Delta(\cdot) = \frac{\partial^2(\cdot)}{\partial x^2} + \frac{\partial^2(\cdot)}{\partial y^2} + \frac{\partial^2(\cdot)}{\partial z^2}$ is the Laplacian operator, $\mathrm{Grad}(\cdot) = \frac{\partial(\cdot)}{\partial x}\mathbf{i} + \frac{\partial(\cdot)}{\partial y}\mathbf{j} + \frac{\partial(\cdot)}{\partial z}\mathbf{k}$ the gradient of a scalar field, $\mathrm{Div}(\cdot) = \frac{\partial(\cdot)}{\partial x} + \frac{\partial(\cdot)}{\partial y} + \frac{\partial(\cdot)}{\partial z}$ the divergence of a vector field, ν the Poisson ratio, μ shear modulus, and $\mathbf{b}$ the body force density.

Field equation (2) is supplemented by kinematic boundary conditions, prescribed at the upper face of the cube

$$u = \frac{\delta_x}{2},\ v = 0,\ w = 0, \tag{3}$$

$$\text{for}\,\forall(x, y, z) : y = a \ \text{ and}\, x, z \in [-a, a],$$

and at the lower face

$$u = -\frac{\delta_x}{2},\ v = 0,\ w = 0, \tag{4}$$

$$\text{for}\,\forall(x, y, z) : y = -a \ \text{ and}\, x, z \in [-a, a],$$

and by static boundary conditions requiring that the lateral surface of the cube be traction-free

$$\mathbf{t} = \mathbf{T}\,\mathbf{n}_{\mathrm{L}} = \boldsymbol{o}, \tag{5}$$

$$\text{for}\,\forall(x,\ y,\ z) : x = \pm a,\ \ \text{and}\ y, z \in [-a,\ a]\,,$$

$$\text{for}\,\forall(x,\ y,\ z) : z = \pm a\ \ \text{and}\ x, y \in [-a,\ a]\,,$$

where $\mathbf{t}$ denotes the Cauchy stress vector, $\mathbf{T}$ the Cauchy stress tensor, and $\mathbf{n}_{\mathrm{L}}$ the outward unit normal to the four faces of the lateral surface. In terms of stress components of tensor $\mathbf{T}$,

$$[\mathbf{T}] = \begin{bmatrix} \sigma_x & \tau_{xy} & \tau_{xz} \\ \tau_{xy} & \sigma_y & \tau_{yz} \\ \tau_{xz} & \tau_{yz} & \sigma_z \end{bmatrix}, \tag{6}$$

conditions on the lateral surface (5) can be rewritten as

$$\sigma_x(\pm a,\ y,\ z) = \tau_{xy}(\pm a,\ y,\ z) = \tau_{xz}(\pm a,\ y,\ z) = 0,\ \text{for}\ y, z \in [-a,\ a]\,, \tag{7}$$

$$\tau_{xz}(x,\ y, \pm a) = \tau_{yz}(x,\ y, \pm a) = \sigma_z(x,\ y, \pm a) = 0,\ \text{for}\ x, y \in [-a,\ a]\,. \tag{8}$$

Field equations (2) and boundary conditions (3), (4), (7), and (8) formalize the equilibrium boundary value problem for a cube subjected to sliding shear.

3 Displacement Field

In the literature there exist several solution representation forms of a linear elastic problem, in terms of displacement, as formulated by the field equation (2). As an example, the solutions of Galerkin, Boussinesq, Papkovitch, and Neuber can be cited [25, 26]. However, having available solution representation forms does not greatly facilitate the resolution of specific problems, the difficulty of which remains substantially connected to the complexity of the boundary conditions to be satisfied. The boundary conditions of the sliding shear problem are not easy to address as they are of a mixed nature.

Given the complexity of our three-dimensional problem, and the absence of formal solutions to similar problems in the literature, some simplifying assumptions about the displacement field must necessarily be introduced. On the basis of experimental and numerical investigations, it can be observed that, for the material points of the body, the displacement component v is small as compared to the component u and that the component w is very small compared to the component u.[1] Moreover, other specific observations can be made in order to solve (2), rewritten below in scalar form and in the absence of body forces

$$\begin{cases} \Delta u + \frac{1}{1-2\nu}\frac{\partial}{\partial x}\left(\frac{\partial u}{\partial x} + \frac{\partial v}{\partial y} + \frac{\partial w}{\partial z}\right) = 0 \\ \Delta v + \frac{1}{1-2\nu}\frac{\partial}{\partial y}\left(\frac{\partial u}{\partial x} + \frac{\partial v}{\partial y} + \frac{\partial w}{\partial z}\right) = 0 \\ \Delta w + \frac{1}{1-2\nu}\frac{\partial}{\partial z}\left(\frac{\partial u}{\partial x} + \frac{\partial v}{\partial y} + \frac{\partial w}{\partial z}\right) = 0 \end{cases}. \tag{9}$$

[1] Indicatively, considering the maximum values, $v/u \simeq 0.3$ and $w/u \simeq 0.03$ (cf. Fig. 3).

Since the boundary conditions do not depend on the variable z, the displacement components u and v show very weak dependence on this variable. In addition to being small itself, the displacement component w also shows a very small (though strictly non-zero) derivative $\partial w/\partial z$ as compared to $\partial u/\partial x$ and $\partial v/\partial y$. Therefore, to derive the displacement field generated by the sliding shear, two kinematic assumptions are formulated.

1. All planes parallel to the middle plane (that is the xy plane passing through the origin G, with equation $z = 0$) exhibit the same in-plane displacement field, namely

$$\begin{aligned} u(x, y, 0) &= u(x, y, z) \\ v(x, y, 0) &= v(x, y, z) \end{aligned}, \tag{10}$$

for any $z \in [-a, a]$.

2. Moving away from the middle plane, the out-of-plane displacement $w(x, y, z)$ has a very small derivative with respect to z

$$\frac{\partial w}{\partial z} \ll \left(\frac{\partial u}{\partial x}, \frac{\partial v}{\partial y}\right), \tag{11}$$

for any $x, y, z \in [-a, a]$. The component $w(x, y, z)$ describes how the cube deforms orthogonally to the xy plane due to prescribed displacements $\pm\delta_x/2$. In particular, the middle plane does not warp, $w(x, y, 0) = 0$, and along every line perpendicular to the middle plane the normal strain $\frac{\partial w}{\partial z}$ is very small.

The two above kinematic assumptions will be checked *a posteriori* in Sect. 6.

With these assumptions, the first two equations of system (9) can be decoupled from the third, allowing to determine the two unknown functions $u(x, y)$ and $v(x, y)$ from the following 2D reduced system:

$$\begin{cases} \frac{\partial^2 u}{\partial x^2} + \frac{\partial^2 u}{\partial y^2} + \frac{1}{1-2\nu}\frac{\partial}{\partial x}\left(\frac{\partial u}{\partial x} + \frac{\partial v}{\partial y}\right) = 0, \\ \frac{\partial^2 v}{\partial x^2} + \frac{\partial^2 v}{\partial y^2} + \frac{1}{1-2\nu}\frac{\partial}{\partial y}\left(\frac{\partial u}{\partial x} + \frac{\partial v}{\partial y}\right) = 0, \end{cases} \tag{12}$$

while the third equation of system (9) will be solved separately to obtain the function $w(x, y, z)$

$$\Delta w + \frac{1}{1-2\nu}\frac{\partial}{\partial z}\left(\frac{\partial u}{\partial x} + \frac{\partial v}{\partial y}\right) = 0. \tag{13}$$

A widely used approach for addressing a broad range of elasticity problems is based on the Fourier method [27]. This technique is typically applied to the governing partial differential equations through separation of variables, superposition, and the use of Fourier series (or Fourier transforms for infinite or semi-infinite domains). For boundary problems in the theory of elasticity, insightful applications of the Fourier series representation method are illustrated in the classical work by Pickett [28]. Discussions about the robustness of Fourier method, with regard to completeness and convergence, can be found in a variety of references (see, for example, [29, 30], and [31]). Applying this solution method, namely using the method of separation of variables and series representation for unknown functions $u(x, y)$, $v(x, y)$, and $w(x, y, z)$, system (12) and equation (13) are satisfied by the following displacement field:

$$
\begin{aligned}
u(x,y) = {} & \frac{\delta_x y}{2a} + \sum_{n=1}^{\infty} \cos\left(\frac{\pi n x}{2a}\right)\left[\cosh\left(\frac{\pi n y}{2a}\right)(A_n + yC_n) + \sinh\left(\frac{\pi n y}{2a}\right)(B_n + yD_n)\right] + \\
& \sum_{m=1}^{\infty} \sin\left(\frac{\pi m y}{2a}\right)\left[\cosh\left(\frac{\pi m x}{2a}\right)(E_m + xG_m) + \sinh\left(\frac{\pi m x}{2a}\right)(F_m + xH_m)\right] + \\
& \sum_{p=1}^{\infty} \sin\left(\frac{\pi p x}{2a}\right)\left[\cosh\left(\frac{\pi p y}{2a}\right)\left(I_p + yM_p\right) + \sinh\left(\frac{\pi p y}{2a}\right)\left(L_p + yN_p\right)\right] + \\
& \sum_{q=1}^{\infty} \cos\left(\frac{\pi q y}{2a}\right)\left[\cosh\left(\frac{\pi q x}{2a}\right)\left(O_q + xQ_q\right) + \sinh\left(\frac{\pi q x}{2a}\right)\left(P_q + xR_q\right)\right], \\
v(x,y) = {} & \sum_{n=1}^{\infty} \sin\left(\frac{\pi n x}{2a}\right)\frac{1}{\pi n}\left[\sinh\left(\frac{\pi n y}{2a}\right)(2a(4\nu-3)D_n + \pi n A_n + \pi n y C_n) + \right. \\
& \left. \cosh\left(\frac{\pi n y}{2a}\right)(2a(4\nu-3)C_n + \pi n B_n + \pi n y D_n)\right] + \\
& \sum_{m=1}^{\infty} \cos\left(\frac{\pi m y}{2a}\right)\frac{1}{\pi m}\left[\sinh\left(\frac{\pi m x}{2a}\right)(2a(3-4\nu)H_m + \pi m E_m + \pi m x G_m) + \right. \\
& \left. \cosh\left(\frac{\pi m x}{2a}\right)(2a(3-4\nu)G_m + \pi m F_m + \pi m x H_m)\right] + \\
& -\sum_{p=1}^{\infty} \cos\left(\frac{\pi p x}{2a}\right)\frac{1}{\pi p}\left[\sinh\left(\frac{\pi p y}{2a}\right)\left(2a(4\nu-3)N_p + \pi p I_p + \pi p y M_p\right) + \right. \\
& \left. \cosh\left(\frac{\pi p y}{2a}\right)\left(2a(4\nu-3)M_p + \pi p L_p + \pi p y N_p\right)\right] + \\
& -\sum_{q=1}^{\infty} \sin\left(\frac{\pi q y}{2a}\right)\frac{1}{\pi q}\left[\sinh\left(\frac{\pi q x}{2a}\right)\left(2a(3-4\nu)R_q + \pi q O_q + \pi q x Q_q\right) + \right. \\
& \left. \cosh\left(\frac{\pi q x}{2a}\right)\left(2a(3-4\nu)Q_q + \pi q P_q + \pi q x R_q\right)\right], \\
w(x,y,z) = {} & \sum_{\substack{n=1,\\ m=1}}^{\infty}\left[S_{n,m}\cosh\left(\frac{\pi\sqrt{1-2\nu}\sqrt{m^2+n^2}}{2\sqrt{2a}\sqrt{1-\nu}}z\right) + \right. \\
& \left. T_{n,m}\sinh\left(\frac{\pi\sqrt{1-2\nu}\sqrt{m^2+n^2}}{2\sqrt{2a}\sqrt{1-\nu}}z\right)\right]\cdot\sin\left(\frac{n\pi x}{2a}\right)\sin\left(\frac{m\pi y}{2a}\right),
\end{aligned}
\tag{14}
$$

where all constants $A \div T$ must be determined by fulfilling the boundary conditions.

According to the deformed shape of the cube under sliding shear, several constants in (14) can be removed, imposing the following symmetry conditions:

$$
\begin{aligned}
u(x,y) &= -u(-x,-y) = u(-x,y) = -u(x,-y) \\
v(x,y) &= -v(-x,-y) = -v(-x,y) = v(x,-y) \\
w(x,y,z) &= -w(x,y,-z) = -w(x,-y,z) = w(-x,-y,z)
\end{aligned}
\quad . \tag{15}
$$

These conditions imply

$$
A_n = D_n = F_m = G_m = I_p = L_p = M_p = N_p = O_q = P_q = Q_q = R_q = S_{r,s} = 0. \tag{16}
$$

In addition, the index m must be even in the coefficients $T_{n,m}$ to satisfy a priori the kinematic boundary conditions $w(x, y, \pm a) = 0$.

Therefore, the displacement field (14) ultimately turns out to be

$$
\begin{aligned}
u(x, y) &= \frac{\delta_x y}{2a} + \sum_{n=1}^{\infty} \cos\left(\frac{\pi n x}{2a}\right)\left[B_n \sinh\left(\frac{\pi n y}{2a}\right) + y C_n \cosh\left(\frac{\pi n y}{2a}\right)\right] + \\
&\sum_{m=1}^{\infty} \sin\left(\frac{\pi m y}{2a}\right)\left[E_m \cosh\left(\frac{\pi m x}{2a}\right) + x H_m \sinh\left(\frac{\pi m x}{2a}\right)\right], \\
v(x, y) &= \sum_{n=1}^{\infty} \sin\left(\frac{\pi n x}{2a}\right) \frac{1}{\pi n}\left[\cosh\left(\frac{\pi n y}{2a}\right)(-2(3-4\nu) a C_n + \pi n B_n)\right. \\
&\left. + \pi n y C_n \sinh\left(\frac{\pi n y}{2a}\right)\right] + \\
&\sum_{m=1}^{\infty} \cos\left(\frac{\pi m y}{2a}\right) \frac{1}{\pi m}\left[\sinh\left(\frac{\pi m x}{2a}\right)(2(3-4\nu) a H_m + \pi m E_m) + \pi m x H_m \cosh\left(\frac{\pi m x}{2a}\right)\right], \\
w(x, y, z) &= \sum_{\substack{r=1,\\ s=2,}}^{\infty} T_{r,s} \sinh\left(\frac{\pi\sqrt{1-2\nu}\sqrt{r^2+s^2}}{2\sqrt{2a}\sqrt{1-\nu}} z\right) \sin\left(\frac{r\pi x}{2a}\right) \sin\left(\frac{s\pi y}{2a}\right).
\end{aligned}
\tag{17}
$$

In the displacement field (17), the only homogeneous contribution $\delta_x y/2a$ has been explicitly separated from the remaining overall inhomogeneous part. Inhomogeneous terms of (17) govern a variable deformation field in the cube, while the homogeneous term characterizes a spatially constant deformation. Specifically, this homogeneous term transforms the initial cube into an oblique parallelepiped, whose sides are parallel two by two (cf. Fig. 2). In the literature, this type of deformation is known as *simple shear* and is represented by the following displacement field:

$$
\begin{aligned}
u(x, y, z) &= \frac{\delta_x}{2a} y \\
v(x, y, z) &= 0 \\
w(x, y, z) &= 0
\end{aligned}
\quad .
\tag{18}
$$

In the case of simple shear, the mathematical formulation of the problem is considerably simplified. In particular, the local equilibrium equations (9) are automatically satisfied.

4 Stress Field

Based on the displacement field (17), the linear Navier constitutive law

$$
\mathbf{T} = 2\mu\mathbf{E} + \lambda\theta\mathbf{I},
\tag{19}
$$

where μ and λ are the Lamé constants, $\mathbf{E} = \frac{1}{2}\left(\mathbf{H} + \mathbf{H}^T\right)$ is the strain tensor, that is the symmetric part of the displacement gradient $\mathbf{H}$, $\theta = \mathrm{tr}\mathbf{E}$, and $\mathbf{I}$ denotes the unit tensor, provides the following stress components:

$$
\sigma_x(x, y, z) = -\frac{\mu}{a} \sum_{n=1}^{\infty}\left[\pi n B_n \sin\left(\frac{\pi n x}{2a}\right) \sinh\left(\frac{\pi n y}{2a}\right) + C_n \sin\left(\frac{\pi n x}{2a}\right) \cdot\right.
$$

$$\left(4a\nu\sinh\left(\frac{\pi ny}{2a}\right)+\pi ny\cosh\left(\frac{\pi ny}{2a}\right)\right)\Bigg]+$$

$$\sum_{m=1}^{\infty}\Bigg[-\pi mE_m\sinh\left(\frac{\pi mx}{2a}\right)\sin\left(\frac{\pi my}{2a}\right)-(2-4\nu)\,aH_m\sinh\left(\frac{\pi mx}{2a}\right)\sin\left(\frac{\pi my}{2a}\right)+$$

$$-\pi mxH_m\cosh\left(\frac{\pi mx}{2a}\right)\sin\left(\frac{\pi my}{2a}\right)\Bigg]+$$

$$-\sum_{\substack{r=1,\\ s=2}}^{\infty}\frac{\pi\mu\nu\sqrt{r^2+s^2}T_{r,s}\sin\left(\frac{\pi rx}{2a}\right)\sin\left(\frac{\pi sy}{2a}\right)\cosh\left(\frac{\pi\sqrt{1-2\nu}\sqrt{r^2+s^2}}{2\sqrt{2}a\sqrt{1-\nu}}z\right)}{\sqrt{2}a\sqrt{1-\nu}\sqrt{1-2\nu}},$$

$$\sigma_y(x,y,z)=\frac{\mu}{a}\sum_{n=1}^{\infty}\Bigg[\pi nB_n\sin\left(\frac{\pi nx}{2a}\right)\sinh\left(\frac{\pi ny}{2a}\right)+C_n\sin\left(\frac{\pi nx}{2a}\right)\cdot$$

$$\left(4a(\nu-1)\sinh\left(\frac{\pi ny}{2a}\right)+\pi ny\cosh\left(\frac{\pi ny}{2a}\right)\right)\Bigg]+$$

$$\sum_{m=1}^{\infty}\Bigg[-\pi mE_m\sinh\left(\frac{\pi mx}{2a}\right)\sin\left(\frac{\pi my}{2a}\right)-(6-4\nu)\,aH_m\sinh\left(\frac{\pi mx}{2a}\right)\sin\left(\frac{\pi my}{2a}\right)+$$

$$-\pi mxH_m\cosh\left(\frac{\pi mx}{2a}\right)\sin\left(\frac{\pi my}{2a}\right)\Bigg]+$$

$$-\sum_{\substack{r=1,\\ s=2,}}^{\infty}\frac{\pi\mu\nu\sqrt{r^2+s^2}T_{r,s}\sin\left(\frac{\pi rx}{2a}\right)\sin\left(\frac{\pi sy}{2a}\right)\cosh\left(\frac{\pi\sqrt{1-2\nu}\sqrt{r^2+s^2}}{2\sqrt{2}a\sqrt{1-\nu}}z\right)}{\sqrt{2}a\sqrt{1-\nu}\sqrt{1-2\nu}},$$

$$\sigma_z(x,y,z)=-4\mu\nu\sum_{n=1}^{\infty}C_n\sin\left(\frac{\pi nx}{2a}\right)\sinh\left(\frac{\pi ny}{2a}\right)+$$

$$-\sum_{m=1}^{\infty}H_m\sinh\left(\frac{\pi mx}{2a}\right)\sin\left(\frac{\pi my}{2a}\right)+$$

$$\sum_{\substack{r=1,\\ s=2,}}^{\infty}\frac{\pi\sqrt{r^2+s^2}\sqrt{1-\nu}\,T_{r,s}\sin\left(\frac{\pi rx}{2a}\right)\sin\left(\frac{\pi sy}{2a}\right)\cosh\left(\frac{\pi\sqrt{1-2\nu}\sqrt{r^2+s^2}}{2\sqrt{2}a\sqrt{1-\nu}}z\right)}{4a\nu\sqrt{2-4\nu}},$$

$$\tau_{xy}(x,y,z)=\frac{\mu}{2a}\delta_x+\frac{\mu}{2a}\sum_{n=0}^{\infty}\Bigg[2\pi nB_n\cos\left(\frac{\pi nx}{2a}\right)\cosh\left(\frac{\pi ny}{2a}\right)+2C_n\cos\left(\frac{\pi nx}{2a}\right)\cdot$$

$$\left(2a(2\nu-1)\cosh\left(\frac{\pi ny}{2a}\right)+\pi ny\sinh\left(\frac{\pi ny}{2a}\right)\right)\Bigg]+$$

$$\sum_{m=1}^{\infty}\Bigg[2\pi mE_m\cosh\left(\frac{\pi mx}{2a}\right)\cos\left(\frac{\pi my}{2a}\right)+8a(1-\nu)\,H_m\cosh\left(\frac{\pi mx}{2a}\right)\cos\left(\frac{\pi my}{2a}\right)+$$

$$2\pi m x H_m \sinh\left(\frac{\pi m x}{2a}\right)\cos\left(\frac{\pi m y}{2a}\right)\Big],$$

$$\tau_{xz}(x,y,z)=\sum_{\substack{r=1,\\ s=2,}}^{\infty}\frac{\pi\mu r\, T_{r,s}\cos\left(\frac{\pi r x}{2a}\right)\sin\left(\frac{\pi s y}{2a}\right)\sinh\left(\frac{\pi\sqrt{1-2\nu}\sqrt{r^2+s^2}}{2\sqrt{2}a\sqrt{1-\nu}}z\right)}{2a},$$

$$\tau_{yz}(x,y,z)=\sum_{\substack{r=1,\\ s=2,}}^{\infty}\frac{\pi\mu s\, T_{r,s}\sin\left(\frac{\pi r x}{2a}\right)\cos\left(\frac{\pi s y}{2a}\right)\sinh\left(\frac{\pi\sqrt{1-2\nu}\sqrt{r^2+s^2}}{2\sqrt{2}a\sqrt{1-\nu}}z\right)}{2a}. \tag{20}$$

For simple shear, once the gradient of the displacement field (18) and the strain tensor have been calculated, the constitutive law (19) gives the following stress tensor:

$$[\mathbf{T}]=\begin{bmatrix}0 & \mu\frac{\delta_x}{2a} & 0\\ \mu\frac{\delta_x}{2a} & 0 & 0\\ 0 & 0 & 0\end{bmatrix}. \tag{21}$$

Tensor (21) shows that only the stress component τ_{xy} is different from zero. This stress component is constant at all points of the body, including its boundary points. Namely, to generate the displacement field (18), which transforms the cube as illustrated in Fig. 2, it is necessary to apply the shear stress τ_{xy} to all points of the four external surfaces of the cube orthogonal to the x and y axes. Under the action of these uniform shear stress distributions, the faces of the cube remain plane. The situation is completely different in the case of the sliding shear problem, where the lateral faces of the cube are kept unloaded. Sliding shear creates an inhomogeneous deformation field (cf. Fig. 1), leaving the lateral faces of the cube traction-free and warped.[2]

5 Setting up of Boundary Conditions

The unknown coefficients $B_n, C_n, E_m, H_m, T_{r,s}$ of the displacement field (17) are determined by imposing both kinematic boundary conditions, (3) and (4), and static boundary conditions, (7) and (8). Operationally, these conditions are imposed pointwise on the lateral surface of the cube through a collocation scheme, obtaining a system of algebraic equations. This system is large and coupled in the unknown constants. Greater accuracy of the numerical evaluations of constants can be obtained by applying the procedure reported in Choudhary et al. [33]. Basically, it consists of imposing boundary conditions in a number of discrete points greater than the number of unknown coefficients. Such an overdetermined system $\mathbf{Ax}=\mathbf{b}$ can be solved by multiplying the coefficient matrix $\mathbf{A}$ and the set of known terms $\mathbf{b}$ by the transpose $\mathbf{A}^{\mathrm{T}}$, thus obtaining a square system $\mathbf{A}^{\mathrm{T}}\mathbf{Ax}=\mathbf{A}^{\mathrm{T}}\mathbf{b}$. This corresponds to applying the least-squares method.

[2]In linear theory, for isotropic materials, the following coaxiality condition holds: $\mathbf{ET}=\mathbf{TE}$, physically based on the coincidence of the principal strain and stress reference systems. Therefore, this condition is also satisfied for both sliding and simple shear. However, unlike the finite theory, it is not possible to establish universal relations [32], that is, relations that hold between strain and stress independently of the constitutive response of the material.

The collocation method consists in imposing the boundary conditions at a given number of points. The optimal collocation points are chosen as the positive roots of the Chebyshev polynomial of first kind of order $(N+1)$ as follows:

$$a\cos\left(\frac{\pi j}{2(N+1)}\right), \quad j=1,2,3,\ldots,N+1. \tag{22}$$

Note that (22) does not include the extrema $\pm a$ as singularities can be expected at the corners of the cube due to the discontinuity of the prescribed displacement. This guarantees the stability of the numerical procedure and a better accuracy of the numerical results.

Operationally, the kinematic boundary conditions (3) and (4) are imposed at nodes y_j according to (22) at one half (for symmetry) of the upper and lower faces of the cube. The static boundary conditions (7) and (8), on the lateral surfaces, are imposed on a half of such surfaces (for symmetry), i.e. on $(0<y\le a,\ -a<z<0)$ and $(0<x\le a,\ -a<y<0)$ at a grid of points (y_j, z_l) and (x_m, y_n), respectively, with $j,n,l,m=1,2,\ldots,2N+1$ and x_m, y_n, y_j, z_l taken according to (22).

Convergence of the method is verified by increasing both N and the number of constants in the series representation (17), and checking the variations of the obtained results in terms of displacements and stress components. It is found that by keeping 5 terms in each series of expression $(17)_{1,2}$, the convergence is achieved. Indeed, it has been checked that further increases of N and/or of the number of collocation points do not lead to a noticeable improvement in the accuracy of the solution.

6 Applications

The method illustrated in the previous Sections is applied below to solve the sliding shear problem. To better illustrate the results, the displacement components were amplified by the factor $10a$, where a is half the side of the cube. Therefore, in the following diagrams, displacements, displacement derivatives, and stresses were multiplied by the same factor. To produce sliding, along the x direction, a horizontal displacement of the upper base relative to the lower base was imposed. This relative displacement is equal to 0.02 times the cube side length $2a$, so that $\delta_x = 0.04a = 0.4\,(10a)$. Consistently with linear theory, a shift δ_x equal to 2% of the cube side can be considered small. The displacement δ_x represents the only external action applied to the cube. As mentioned several times, the lateral faces of the cube were assumed to be traction-free. For definiteness, the Young modulus and Poisson ratio were taken as 2 MPa and 0.1, respectively. The geometric dimension a was set equal to one.

The numerical method presented in Sect. 5 converges rapidly. In fact, the coefficients of each series involved in the displacement $u(x,y)$ and $v(x,y)$ decrease very rapidly as the number of harmonics increases. For the adopted geometric and mechanical parameters, it can be observed that the behavior of these series coefficients is such that there is at least one order of magnitude between a generic coefficient of order n and that of order $n+1$, namely $C_{n+1}/C_n < 10^{-1}$, for almost all coefficients. This makes it possible to limit the number of coefficients in the series. In particular, the series in $(17)_{1,2}$ were truncated to the first 5 harmonics, for a total of 40 coefficients. A similar argument applies to the coefficients of the displacement $w(x,y,z)$. Indeed, for this displacement component, the coefficients $T_{r,s}$ decrease even more rapidly than the coefficients in $(17)_{1,2}$. However, because of the significant variability of $w(x,y,z)$ in planes parallel to the xy plane, maintaining sufficient numerical accuracy required retaining the first 6 harmonics (i.e., $s = 2, 4, \ldots, 12$) for varying values of the first index r, with $r = 1, 2, \ldots, 12$, for a total of 72 coefficients $T_{r,s}$.

The semi-analytical results obtained with the proposed method are compared with those provided by a completely numerical and three-dimensional FE analysis. The numerical model was developed through the software *Straus7* release 2.4.6. The mesh was generated by subdividing a cube, having side length equal to 2 units, into 64,000 cubic 8-node solid brick elements (8-node hexahedra). For simplicity, a uniform geometric partition of the cube was adopted. The numerical scheme implements a conventional isoparametric mapping and polynomial shape functions. To obtain a smoother and more reliable representation of the FE results near the corners, the stress values provided by the numerical model were filtered by excluding the nodes resting in the neighbourhood of the corners. More specifically, the contour lines do not include data related to nodes lying inside spherical regions centered at the corners and having a radius equal to 1/25 of half the side length of the cube.

Using color maps, Fig. 3 shows the results obtained for the displacement field. The displacement component u, in the same direction as the prescribed displacement δ_x, exhibits the largest values (cf. Fig. 3a). While, the displacement component w, parallel to the z axis and orthogonal to u, is characterized by much smaller values (cf. Fig. 3c). The u component is antisymmetric with respect to the x axis and symmetric with respect to the y axis. It is zero along the x axis ($y = 0$) and increases, in absolute value, as it moves toward the upper and lower edges, where it assumes its maximum values equal to $\pm\delta_x/2$ (cf. Fig. 3a). The v component is symmetric with respect to the x axis and antisymmetric with respect to the y axis. It is zero along the y axis ($x = 0$) and increases, in absolute value, as it moves toward the vertical edges, assuming the maximum values in correspondence with the x axis (cf. Fig. 3b). The w component is antisymmetric with respect to both the x and y axes. It shows how the lateral face ($z = a$) of the cube warps (cf. Fig. 3c). Figure 3d displays the deformed profile of the cube's middle plane ($z = 0$) and, given hypothesis (10), of any plane parallel to it. Due to the deformation, the cube's horizontal faces remain flat, rigidly translating parallel to the xz plane, as prescribed by the boundary conditions (3) and (4). The vertical faces ($x = \pm a$), congruent with these rigid horizontal displacements, assume a cylindrical shape with an S-shaped directrix.

In all figures, the FE results are shown by dotted lines. These results agree with those obtained with the proposed method.

In the case of simple shear, unlike sliding shear, the four vertical faces of the cube remain flat. At every point of the cube, both the v and w components are zero, while the u component varies linearly with the variable y.

The purpose of Fig. 4 is to show the comparisons performed with the FEM to check the kinematic hypotheses (10) and (11). The u and v displacement components calculated using the FEM and therefore without introducing hypothesis (10), as pointed out by Figs. 4a and 4b, actually do not show a dependence on variable z, being practically constant along fibers parallel to the z axis. Figures 4c and 4d show that, along two material fibers of the cube (but the same is true for other possible fibers), the derivative $\partial w/\partial z$ is numerically small. Even if this derivative is not strictly zero, hypothesis (11) allows the system (9) to be decoupled.

In Fig. 5, the color maps of the stress distributions in the middle plane $z = 0$ are plotted. The plane distributions of the three normal stresses σ_x, σ_y, σ_z and the shear stress τ_{xy} are illustrated. In this plane, the other two shear stress components τ_{xz} and τ_{yz} are zero due to symmetry. From Fig. 5 it can be seen that the components σ_x, σ_z (cf. Figs. 5a and 5c) are small compared to the components σ_y, τ_{xy} (cf. Figs. 5b and 5d). The normal stress σ_y is zero along the x axis and increases as it moves towards the horizontal edges, reaching its maxima (in absolute value) at the corners. The shear stress τ_{xy} has a parabolic shape

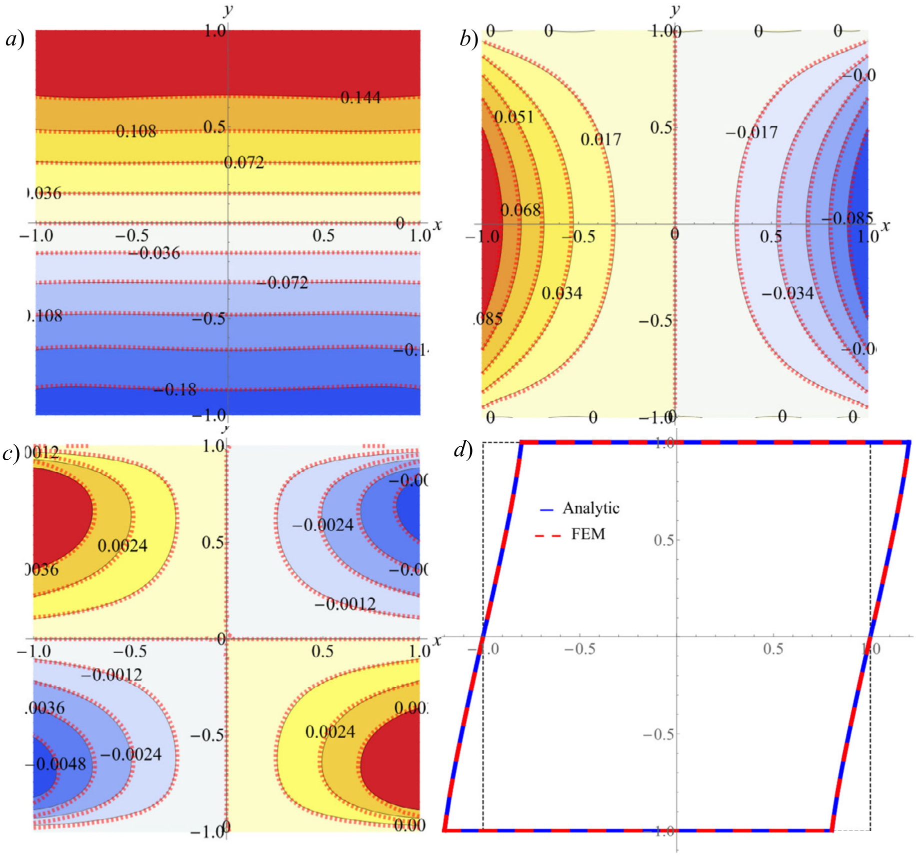

Fig. 3 Displacement field (in [mm]). All numerical values have been amplified by the factor $10a$. (a) Color map of the displacement component $u(x, y)$ for any plane parallel to the middle plane $z = 0$. (b) Color map of the displacement component $v(x, y)$ for any plane parallel to the middle plane $z = 0$. (c) Color map of the displacement component $w(x, y, z)$ for the plane $z = a$. (d) Deformed profile of any cross section of the cube parallel to the middle plane $z = 0$

along the x axis, where it reaches its maximum at the origin, then tends to assume a uniform distribution as it moves toward the horizontal edges. Orthogonally to the middle plane, the stresses undergo small changes, which do not qualitatively change the scenario illustrated by Fig. 5. Ultimately, it can be observed that the sliding shear generates variable stress fields inside the cube, whose important components are τ_{xy} and σ_y. The four lateral faces of the cube are traction-free.

Simple shear generates a uniform stress field characterized by the single shear component $\tau_{xy} = \mu\delta_x/2a$ (cf. (21)). This stress occurs at every internal point of the cube and at every point of the lateral surfaces $x = \pm a$ and $y = \pm a$.

7 Conclusions

The equilibrium boundary value problem for the sliding shear model has been formalized in this paper. Compared to the classic simple shear model, the only difference in the mathe-

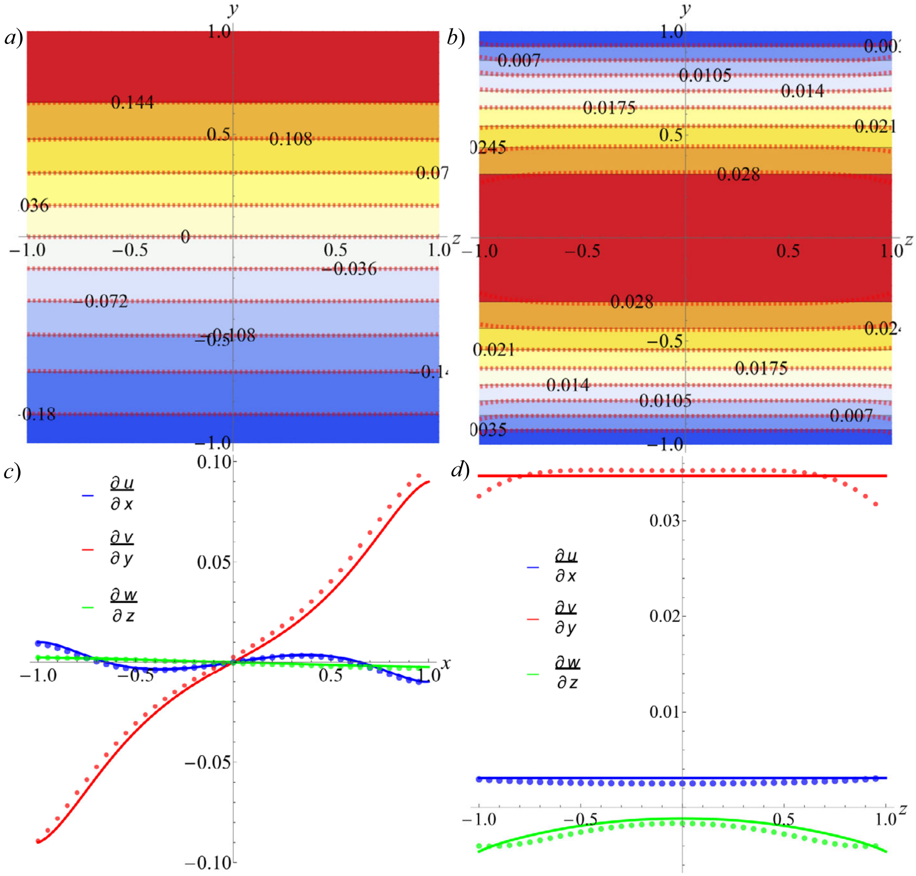

Fig. 4 Verification of kinematic assumptions. All numerical values have been amplified by 10. (a) Color map of the displacement component u in the yz plane ($x = 0$) (in [mm]). (b) Color map of the displacement component v in the yz plane ($x = 0$) (in [mm]). (c) Plot of partial derivatives along the fiber $y = a/2$, $z = 0$, and $-a < x < a$. (d) Plot of partial derivatives along the fiber $x = y = a/2$, and $-a < z < a$

matical formulation lies in different boundary conditions on the lateral surfaces of the solid, since these are assumed to be traction-free. This different boundary condition generates an inhomogeneous displacement field inside the solid (in the simple shear it is homogeneous) and the lateral surfaces warp (in simple shear they remain flat).

By introducing two kinematic assumptions, the field equation has been simplified and the Fourier method was subsequently applied, finding series solutions, containing unknown constants. Obviously, these constants depend on the boundary conditions which, however, are of a mixed nature (i.e., kinematic on the two horizontal faces and static on the four lateral faces), and therefore not easy to handle. To overcome this difficulty and determine the constants, a criterion has been proposed to satisfy the boundary conditions according to a discrete collocation scheme.

Once the constants were calculated, semi-analytical expressions of the displacement and stress fields were obtained. An application was performed on a solid with the shape of a cube, and the results were visualized using 2D color maps. Good agreement was observed between the semi-analytical solution and the three-dimensional FE results. The three scalar

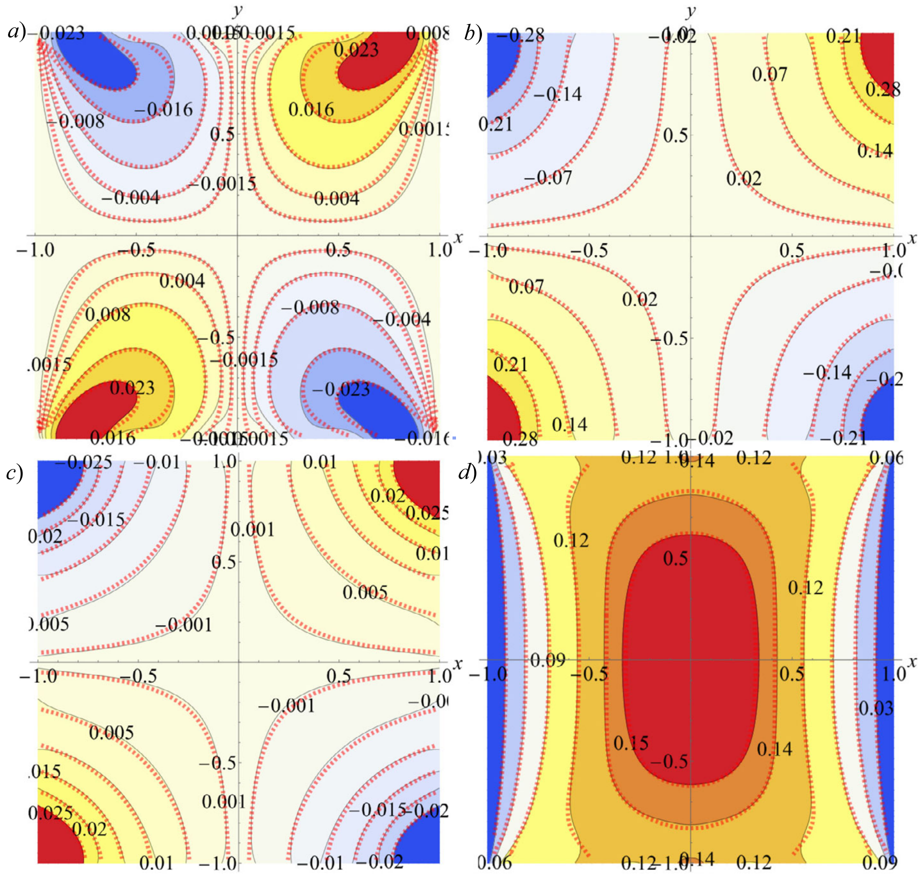

Fig. 5 Stress fields in the middle plane $z = 0$ (in [MPa]). All numerical values have been amplified by the factor 10. (a) Color map of normal stress component σ_x. (b) Color map of normal stress component σ_y. (c) Color map of normal stress component σ_z. (d) Color map of shear stress component τ_{xy}

components of the displacement show different magnitudes and are variable within the cube (in the simple shear there is only one component, the one in the direction of the prescribed displacement, which varies linearly along that direction). Of the six stress components, the three normal stresses and the shear stress directly related to the prescribed displacement were displayed; the other two shear stresses are practically zero (in the simple shear there is only a constant tangential stress).

Author contributions F.O.F.: Theoretical conceptualization, investigation, software, validation. L.L.: data reduction, investigation, writing – review. A.M.T.: visualization, supervision, project administration, funding acquisition.

Funding Information Open access funding provided by Università degli Studi di Modena e Reggio Emilia within the CRUI-CARE Agreement. The Italian Ministry of University and Research (MUR) is gratefully acknowledged for the financial support received through the research project FISA-2022-00183 "Earth-Tech" - Implementation of new Shot-Earth technology in the construction industry, CUP E93C24000250001, and the research grant FIS 2 "Large and offshore deformations of everyday life: from seismic isolators to person's health", project FIS-2023-01661, CUP E53C25000450001. This work was also supported by the Italian

Ministry of University and Research (MUR) through the research grant FIS 2 "PNC-Gen" (project n. FIS-2023-02409; CUP E53C25000440001). Financial support by the National Group of Mathematical Physics (GNFM-INdAM) is also acknowledged.

Data availability No datasets were generated or analysed during the current study.

Declarations

Competing interests The authors declare no competing interests.

References

1. Paulay, T.: The shear strength of shear walls. Bull. N.Z. Soc. Earthqu. Eng. **3**, 148–162 (1970)
2. Colotti, V.: Shear behavior of RC structural walls. J. Struct. Eng. **119**, 728–746 (1993)
3. Hidalgo, P.A., Ledezma, C.A., Jordan, R.M.: Seismic behavior of squat reinforced concrete shear walls. Earthq. Spectra **18**, 287–308 (2002)
4. Coward, M.P., Potts, G.J.: Complex strain patterns developed at the frontal and lateral tips to shear zones and thrust zones. J. Struct. Geol. **5**, 383–399 (1983)
5. Simpson, C., De Paor, D.G.: Strain and kinematic analysis in general shear zones. J. Struct. Geol. **15**, 1–20 (1993)
6. Mukherjee, S., Koyi, H.A.: Higher Himalayan Shear Zone, Sutlej section: structural geology and extrusion mechanism by various combinations of simple shear, pure shear and channel flow in shifting modes. Int. J. Earth Sci. (Geol. Rundsch.) **99**, 1267–1303 (2010)
7. Amirbayat, J., Hearle, J.W.S.: Properties of unit composites as determined by the properties of the interface. Part I: mechanism of matrix-fibre load transfer. Fibre Sci. Technol. **2**, 123–141 (1969)
8. Nunes, L.C.S.: Shear modulus estimation of the polymer polydimethylsiloxane (PDMS) using digital image correlation. Mater. Des. **31**, 583–588 (2010)
9. Dobrzański, P., Oleksiak, W.: Design and analysis methods for composite bonded joints. Trans. Aerosp. Res. **1**, 45–63 (2021)
10. Macefield, V.G., Häger-Ross, C., Johansson, R.S.: Control of grip force during restraint of an object held between finger and thumb: responses of cutaneous afferents from the digits. Exp. Brain Res. **108**, 155–171 (1996)
11. Dzitac, P., Mazid, A.M., Ibrahim, M.Y., Appuhamillage, G.K., Choudhury, T.A.: Friction-based slip detection in robotic grasping. In: IECON 2015 - 41st Annual Conference of the IEEE Industrial Electronics Society, Yokohama, Japan, pp. 4871–4874 (2015). https://doi.org/10.1109/IECON.2015.7392863
12. Zhang, X., Wu, L., He, S., Sha, Z., Huang, Y., Wu, S., Chu, D., Wang, C.H., Peng, S.: Recent advances of slip sensors for smart robotics. Adv. Mater. Technol., e02251 (2026). https://doi.org/10.1002/admt.202502251
13. Todhunter, I., Pearson, K.: A History of the Theory of Elasticity and of the Strength of Materials from Galilei to the Present Time, vol. 1. Cambridge University Press, Cambridge (1886)
14. Vicat, L.: Ponts suspendus en Fil de Fer sur le Rhône. Chez Carilian- Goeury, Paris (1831)
15. Signorini, A.: Trasformazioni termoelastiche finite, rispettivamente: memoria I. Ann. Mat. Pura Appl. **22**, 33–143 (1943)
16. Truesdell, C., Toupin, R.: The classical field theories. In: Flügge, S. (ed.) Encyclopedia of Physics/Handbuch der Physik. Principles of Classical Mechanics and Field Theory, pp. 226–858. Springer, Berlin (1960)
17. Thomson, W., Tait, P.G.: Treatise on Natural Philosophy. Oxford University Press, London (1867)
18. Rivlin, R.S.: Large elastic deformation of isotropic materials. IV. Further developments of the general theory. Philos. Trans. R. Soc. A **241**, 379–397 (1948)

19. Horgan, C.O., Murphy, J.G.: Simple shearing of incompressible and slightly compressible isotropic nonlinearly elastic materials. J. Elast. **98**, 205–221 (2010)
20. Destrade, M., Murphy, J.G., Saccomandi, G.: Simple shear is not so simple. Int. J. Non-Linear Mech. **47**, 210–214 (2012)
21. Nunes, L.C.S., Moreira, D.C.: Simple shear under large deformation: experimental and theoretical analyses. Eur. J. Mech. A Solids **42**, 315–322 (2013)
22. Wang, D., Wu, M.S.: Generalized shear of a soft rectangular block. J. Mech. Phys. Solids **70**, 297–313 (2014)
23. Thiel, C., Voss, J., Martin, R.J., Neff, P.: Shear, pure and simple. Int. J. Non-Linear Mech. **112**, 57–72 (2019)
24. Falope, F.O., Lanzoni, L., Tarantino, A.M.: Shear models in finite elasticity. J. Elast. **158** (2026). https://doi.org/10.1007/s10659-026-10187-3
25. Papkovich, P.F.: Solution Générale des équations differentielles fondamentales d'élasticité exprimée par trois fonctions harmoniques. C. R. Acad. Sci. Paris **195**, 513–515 (1932)
26. Neuber, H.: Ein neuer Ansatz zur Lösung räumlicher Probleme der Elastizitätstheorie. Z. Angew. Math. Mech. **14**, 203–212 (1934)
27. Sadd, M.H.: Elasticity: Theory, Applications, and Numerics. Elsevier, Amsterdam (2005)
28. Pickett, G.: Application of the Fourier method to the solution of certain boundary problems in the theory of elasticity. J. Appl. Mech. **11**, A176–A182 (1944)
29. Timoshenko, S., Goodier, J.N.: Theory of Elasticity, 3rd edn. McGraw–Hill (1970)
30. Little, R.W.: Elasticity. Prentice-Hall (1973)
31. Meleshko, V.V.: Selected topics in the history of the two-dimensional biharmonic problem. Appl. Mech. Rev. **56**, 33–85 (2003)
32. Rivlin, R.S.: Universal relations for elastic materials. Rend. Mat. Appl. **20**, 35–55 (2000)
33. Choudhary, A., Martha, S.C., Chakrabarti, A.: Modified method for the solution of dual trigonometric series relations. Proc. Natl. Acad. Sci. India Sect. A Phys. Sci. **90**, 437–445 (2020)